

High-resolution spectroscopy and abundance analysis of δ Scuti stars near the γ Doradus instability strip

F. Kahraman Alıçavuş^{1,2*}, E. Niemczura², M. Polińska³, K. G. Hełminiak^{4,5},
P. Lampens⁶, J. Molenda-Żakowicz^{2,7}, N. Ukita^{8,9}, E. Kambe⁸

¹Canakkale Onsekiz Mart University, Faculty of Sciences and Arts, Physics Department, 17100, Canakkale, Turkey

²Instytut Astronomiczny, Uniwersytet Wrocławski, ul. Kopernika 11, 51-622 Wrocław, Poland

³Astronomical Observatory Institute, Faculty of Physics, A. Mickiewicz University, Słoneczna, 36, 60-286, Poznań, Poland

⁴Subaru Telescope, National Astronomical Observatory of Japan, Hilo, HI 96720, USA

⁵Department of Astrophysics, Nicolaus Copernicus Astronomical Center, ul. Rabiańska 8, PL-87-100 Toruń, Poland

⁶Royal Observatory of Belgium, Ringlaan 3, B-1180 Brussel, Belgium

⁷Department of Astronomy, New Mexico State University, Las Cruces, NM 88003, USA

⁸Okayama Astrophysical Observatory, National Astronomical Observatory of Japan, 3037-5 Honjo, Kamogata, Asakuchi, Okayama 719-0232, Japan

⁹The Graduate University for Advanced Studies, 2-21-1 Osawa, Mitaka, Tokyo 181-8588, Japan

Accepted ... Received ...; in original form ...

ABSTRACT

δ Scuti stars are remarkable objects for asteroseismology. In spite of decades of investigations, there are still important questions about these pulsating stars to be answered, such as their positions in $\log T_{\text{eff}} - \log g$ diagram, or the dependence of the pulsation modes on atmospheric parameters and rotation. Therefore, we performed a detailed spectroscopic study of 41 δ Scuti stars. The selected objects are located near the γ Doradus instability strip to make a reliable comparison between both types of variables. Spectral classification, stellar atmospheric parameters (T_{eff} , $\log g$, ξ) and $v \sin i$ values were determined. The spectral types and luminosity classes of stars were found to be A1 – F5 and III – V, respectively. The T_{eff} ranges from 6600 to 9400 K, whereas the obtained $\log g$ values are from 3.4 to 4.3. The $v \sin i$ values were found between 10 and 222 km s^{-1} . The derived chemical abundances of δ Scuti stars were compared to those of the non-pulsating stars and γ Doradus variables. It turned out that both δ Scuti and γ Doradus variables have similar abundance patterns, which are slightly different from the non-pulsating stars. These chemical differences can help us to understand why there are non-pulsating stars in classical instability strip. Effects of the obtained parameters on pulsation period and amplitude were examined. It appears that the pulsation period decreases with increasing T_{eff} . No significant correlations were found between pulsation period, amplitude and $v \sin i$.

Key words: stars: general – stars: abundances – stars: chemically peculiar – stars: rotation – stars: variables: δ Scuti

1 INTRODUCTION

Asteroseismology provides a great opportunity to probe the internal structures of stars by modelling their pulsation modes. Many pulsating stars have been examined in detail to determine their pulsational properties. One of the remarkable objects for asteroseismology are δ Scuti (δ Sct) variables because of their large number of pulsation modes, amplitude

regimes, which ranges from low ($\leq 0^m.1$) to high ($\geq 0^m.3$) amplitudes, and their positions in the Hertzsprung-Russell (H-R) diagram.

The δ Sct stars range from dwarf to giant stars and have spectral types between A0 and F5 (Chang et al. 2013). These stars oscillate in radial and non-radial, low-order pressure (p), gravity (g) and mixed modes excited by the κ -mechanism. Most δ Sct stars pulsate in the frequency range from 5 to 50 d^{-1} . Their masses vary between 1.5 and 2.5 M_{\odot} (Chang et al. 2013). The coolest δ Sct stars in the

* E-mail: filizkahraman01@gmail.com/filizkahraman@comu.edu.tr

δ Sct instability strip are in the transition region, where the convective envelope gradually turns into a radiative one, and the energy is transferred by convection in the core (Aerts, Christensen-Dalsgaard, & Kurtz 2010, Section 3.7.3). Investigations of δ Sct stars will help us to understand processes occurring in the transition region.

δ Sct variables are located in the lower part of the classical instability strip where the theoretical instability strips of δ Sct and γ Doradus (γ Dor) variables partially overlap. In this overlapping area, δ Sct/ γ Dor hybrids were predicted observationally (Breger & Beichbuchner 1996; Handler & Shobbrook 2002) and theoretically (Dupret et al. 2004). The number of these variables increased with the discoveries based on space telescopes observations. Thanks to the high precision photometry obtained by the *Kepler* space telescope, many δ Sct, γ Dor, and candidate hybrid stars have been discovered (Uytterhoeven et al. 2011; Grigahcène et al. 2010). Uytterhoeven et al. (2011) showed the position of δ Sct, γ Dor, and candidate hybrid stars in the H-R diagram mainly by using the photometric atmospheric parameters taken from the *Kepler* input catalog (KIC) (Brown et al. 2011). It turned out that δ Sct and γ Dor stars can be found outside their theoretical instability strips. The candidate hybrid stars have been discovered in the instability strip of the δ Sct as well as γ Dor stars. To find out the exact positions of δ Sct and the other A-F type pulsating stars, spectroscopic studies are essential.

Some detailed spectroscopic studies dealing with these variables have been carried out (Catanzaro et al. 2011; Tkachenko et al. 2013; Niemczura et al. 2015; Kahraman Aliçavuş et al. 2016). The atmospheric parameters and the abundance patterns of δ Sct, γ Dor, and hybrid stars were derived and their accurate positions in the $\log T_{\text{eff}} - \log g$ have been determined. According to these studies, δ Sct stars were found mainly inside their theoretical instability strip. A detailed abundance pattern of the δ Sct stars was investigated by Fossati et al. (2008) to check whether the assumption of solar abundance in the pulsation models was correct. They found that generally the elements Y and Ba are overabundant. The abundance pattern of δ Sct stars were also compared with the non-pulsating A-F type stars and no significant differences were found. However, it should be kept in mind that only few δ Sct stars were used in this study.

On the other hand, a lot of studies based on the frequency analysis of δ Sct stars were presented. For instance, Balona & Dziembowski (2011) and Balona (2014) examined the pulsation frequencies of δ Sct stars using the *Kepler* data. They showed that the δ Sct stars beyond the blue edge of their instability strip pulsate in high-radial and non-radial overtones as suggested by Breger & Bregman (1975). The authors tested the working hypothesis that rotation in connection with stellar spots (i.e. rotational modulation) could explain the low frequencies but conclude that “rotational splitting, by itself, cannot account for the number of low frequencies nor their distribution”. In the study of Balona & Dziembowski (2011) a gap between zero age main sequence (ZAMS) and the position of δ Sct stars in the H-R diagram was also found. It was shown that the gap increases with growing effective temperature.

Although much is already known about their stellar properties, several big issues concerning δ Sct stars are still

unanswered. For example, the exact position of δ Sct stars in the H-R diagram and borders of their instability strip need to be checked observationally. Additionally, δ Sct stars in the red border of their instability strip have almost the same atmospheric parameters as γ Dor stars but pulsate in different modes. It is known that chemical composition influences the opacity in stars and opacity is related to the κ mechanism. Additionally, it is known that the chemical composition affects the pulsation modes (Miglio et al. 2008). Therefore, this situation could be explained by a possible chemical abundance differences between δ Sct and γ Dor stars. The other question concerns the relation between the pulsation quantities and rotation and metallicity of δ Sct stars.

To answer all these questions detailed spectroscopic studies of δ Sct stars are necessary, preferably using high-resolution observations. Hence, in this study, we aim to obtain fundamental atmospheric parameters and chemical composition of a sample of δ Sct stars based on high-resolution spectra taken with different instruments. We have selected a sample of 41 δ Sct stars from the catalogue of Rodríguez, López-González, & López de Coca (2000). 31 of these stars are confirmed δ Sct variables and the others are suspected δ Sct variables which show pulsation but do not have reliable photometric studies to confirm δ Sct type variability.

Stars were selected considering their position in the H-R diagram. The δ Sct stars located in/near the overlapping region of δ Sct and γ Dor instability strips were chosen. In Sect. 2 details of the observations and data reductions are given. Spectral classification of stars is presented in the Sect. 3. Determinations of initial atmospheric parameters from photometric indices of several systems and from spectral energy distribution are introduced in Sect. 4. In Sect. 5, the spectroscopic determination of atmospheric parameters and chemical abundances are given. Discussion of the results and conclusions are presented in Sect. 6 and Set. 7, respectively.

2 OBSERVATIONS

In our analysis, we used high-resolution spectra taken with four spectrographs: ARCÉS, ELODIE, HERMES and HIDES. The information about the spectroscopic survey is given in Table 1. The signal-to-noise (S/N) ratios of the spectra near the wavelength 5500 Å are listed in Table 2.

The ARC Échelle Spectrograph (ARCÉS) is a high-resolution, cross-dispersed optical spectrograph mounted at the 3.5-m telescope of the Apache Point Observatory (USA). It captures the entire spectrum between 3200 and 10000 Å in a single exposure. ARCÉS provides spectra with a resolving power of $R \sim 31\,500$. For the reduction of the data, we used the NOAO/IRAF¹ package and the procedure described in the ARCÉS data reduction cookbook². The reduction process included the bias subtraction, bad pixels fixing, trimming, scattered light correction, removal of the cosmic rays, flat-field correction and calibration in wavelength done on

¹ <http://iraf.noao.edu/>

² The ARCÉS Data Reduction Cookbook by Karen Kinemuchi is available at the website [http://astronomy.nmsu.edu:8000/apo-wiki/wiki/ARCÉS no1](http://astronomy.nmsu.edu:8000/apo-wiki/wiki/ARCÉS%20no1).

Table 1. Information about the spectroscopic survey. N gives the number of observed stars.

Instrument	N	Observations years	Resolving power	Spectral range [Å]
ARCES	4	2015	31500	3850 – 10500
ELODIE	8	1999 – 2004	42000	3900 – 6800
HERMES	6	2015	85000	3770 – 9000
HIDES	23	2015	50000	4080 – 7525

the basis of the exposures of the ThAr calibration lamps. The spectra were extracted with the use of the *apall* task also provided by IRAF.

ELODIE is a cross-dispersed échelle spectrograph used at the 1.93-m telescope of Observatoire de Haute Provence (OHP, France) between late 1993 and mid 2006. The spectra cover the wavelength range from 3850 to 6800 Å with a resolving power of 42000. The standard data reduction of the ELODIE data was performed automatically with the dedicated pipeline. The reduced archival ELODIE data were taken from the public archive³ (Moultaka et al. 2004).

The High Efficiency and Resolution Mercator Échelle Spectrograph (HERMES) is a high-resolution fibre-fed échelle spectrograph attached to the 1.2-m Mercator telescope at the Roque de los Muchachos Observatory (ORM, La Palma, Spain) (Raskin et al. 2011). The spectra acquired in the high-resolution fiber have a resolving power $R \sim 85\,000$ and cover the spectral range from 3770 to 9000 Å. The data have been reduced with a dedicated pipeline⁴, which includes bias subtraction, extraction of scattered light, cosmic ray filtering, wavelength calibration by a ThArNe lamps and order merging.

The High-Dispersion Échelle Spectrograph (HIDES Izumiura 1999) is attached to the 1.88-m telescope of the Okayama Astrophysical Observatory (Japan). The spectra cover the visual wavelength range with the resolving power $R \sim 50\,000$ with its high-efficiency fiber-link (Kambe et al. 2013). The reduction was made using dedicated IRAF-based scripts that deal with all chips simultaneously, and included bias, flat-field, and scattered light subtraction, corrections for bad pixels and cosmic rays, aperture extraction, and wavelength calibration. The last step was done on the basis of ThAr lamp exposures. Spectra from three chips were later merged into one file. Due to crowding of the apertures and sudden drop in the signal from the bluest chip, we have extracted only the 24 reddest orders. The final product is composed of 62 spectral orders, spanning from 4080 to 7520 Å. A more detailed description of the data reduction process is given in Helminiak et al. (2016).

The normalisation of spectra was performed manually using the *continuum* task of the NOAO/IRAF package. The spectra were divided into several parts and each part was normalised individually. The normalisation was checked by comparing the observed spectrum with a synthetic spectrum assuming an approximate effective temperature (T_{eff}), surface gravity ($\log g$) and projected rotational velocity ($v \sin i$) values. Because of limited observation time, typically one spectrum was obtained per star. However, line profiles in

each spectrum were checked carefully to be sure whether the spectroscopic double-lined binary (SB2) stars are present in our sample. A few suspect SB2 stars were found (GW Dra, EE Cam, V1162 Ori, and GX Peg) and excluded from the further analysis. In the case of multiple spectra available for a star, we investigated the averaged spectrum. The averaging process was applied after normalisation.

3 SPECTRAL CLASSIFICATION

Stellar spectral types and luminosity classes were obtained by using the classical spectral classification method (Gray & Corbally 2009) of comparison spectra of the studied stars with those of standards (Gray et al. 2003). Our sample consists of A and F stars, so the spectral types are typically derived from hydrogen H δ and H γ , Ca II K, and metal lines. For non-chemically peculiar (non-CP) objects, all these lines provide the same spectral type. These lines are available only in the spectra taken with HERMES. In addition, the hydrogen lines are an excellent tool to derive luminosity types of A stars, but the sensitivity to the luminosity decreases in late A type stars and the ionised metal lines become useful (Gray & Corbally 2009). Therefore, the luminosity class was obtained from the hydrogen lines for early A stars, whereas for later types the lines of ionised Fe and Ti were used.

Spectral types of the analysed stars were derived in the range from A1 to F5, and luminosity classes from III to V. For some objects, spectral classification was difficult because of the available spectral range and normalisation problems occurring typically in broad Balmer lines. The normalisation problem was caused by the merging of short orders in the ARCES and HIDES spectra. Additionally, the spectral range of HIDES data starts around 4080 Å, therefore the analysis of Ca II H and K lines, as well as the H δ line was impossible for the spectra taken with this instrument. The literature and new spectral classes of the investigated stars are shown in Table 2.

4 ATMOSPHERIC PARAMETERS FROM PHOTOMETRY AND SPECTRAL ENERGY DISTRIBUTION

Initial atmospheric parameters, T_{eff} and $\log g$ were obtained from the photometric indices and the spectral energy distribution (SED). These parameters were used as inputs in the subsequent spectral analysis.

The interstellar reddening, $E(B - V)$, has a notable influence on the values of atmospheric parameters determined by photometric indices. Hence, the $E(B - V)$ value should be taken into account in the analysis. First, we derived $E(B - V)$ values using an interstellar extinction map and NaD₂ interstellar line. The $E(B - V)$ values were first determined from the interstellar extinction map (Amôres & Lépine 2005) using the Galactic coordinates and distances of targets. We used the HIPPARCOS parallaxes (van Leeuwen 2007) for the stars which have distances less than 100 parsec and Gaia parallaxes (Casertano et al. 2017) for the stars which have distances

³ <http://atlas.obs-hp.fr/elodie/>

⁴ <http://hermes-as.oma.be/doxygen/html/index.html>

Table 2. Information about the investigated stars.

HD number	Name	Instrument	S/N	V (mag)	Sp. type (Simbad)	Sp. type (this study)
089843 ^{a,1}	EN UMa	ARCES	210	5.90	A7 Vn	A6 V
099002	CX UMa	ARCES	190	6.94	F0	A7 V
115308	DK Vir	ARCES	220	6.69	F1 IV	F2 V
	*EH Lib	ARCES	150	9.83	A5	A7 V
010088		ELODIE	115	7.86	A0	F0 V
012389		ELODIE	100	7.98	A0	A5 IV
023156	V624 Tau	ELODIE	190	8.22	A7 V	A6 V
062437	AZ CMi	ELODIE	220	6.47	F0 III	A7 IV
073857	*VZ Cnc	ELODIE	70	7.18	A9 III	F2 III
103313	IQ Vir	ELODIE	230	6.31	F0 V	A6 V
110377	GG Vir	ELODIE	210	6.22	A6 Vp	A5 IV
191635	**V2109 Cyg	ELODIE	140	7.49	F0	F5 IV
192871	*V383 Vul	HERMES	180	7.51	F1 V(n)	F2 IV
199908	DQ Cep	HERMES	175	7.26	F1 IV	F2 V
210957		HERMES	160	8.00	A9 IV	A6 V
213272 ^{a,2}	*	HERMES	180	6.55	A2 V	A1 IV
214698 ^{a,3}	41 Peg	HERMES	200	6.33	A2 V	A1 IV
219586 ^{a,4}	V388 Cep	HERMES	160	5.55	F0 IV	F1 IV
034409	BS Cam	HIDES	100	8.43	F2	F2 IV
037819	V356 Aur	HIDES	130	8.08	F8	hF3mF6 III
050018	OX Aur	HIDES	90	6.10	F2 Ve	F2 IV
060302 ^{a,5}	V344 Gem	HIDES	80	8.02	F0	F0 IV
079781	GG UMa	HIDES	100	8.59	F5	hF0mF3 III
081882	KZ UMa	HIDES	130	8.12	F0	A9 V
082620	DL UMa	HIDES	170	7.18	F0	F2 V
084800	IX UMa	HIDES	170	7.90	A2 II	A1 V
090747 ^{a,6}	GS UMa	HIDES	85	8.66	F8	F4 IV
093044	EO UMa	HIDES	135	7.11	A7 III	F0 V
097302	FI UMa	HIDES	70	6.64	A4 V	A4 IV
099983	HQ UMa	HIDES	120	7.10	F0	F2 IV
102355	KW UMa	HIDES	80	6.60	F0	A2 IV
118954 ^{a,5}	IP UMa	HIDES	110	7.66	A5	F2 V
127411	IT Dra	HIDES	140	7.52	A2	A2 V/IV
151938	V919 Her	HIDES	120	8.35	F2	F3 IV
154225	V929 Her	HIDES	120	7.96	A5m	F2 V
155118	V873 Her	HIDES	100	8.40	F0	F3 III
161287	V966 Her	HIDES	100	7.98	F2	F1 IV
176445	V1438 Aql	HIDES	80	7.72	F0	F3 III
176503 ^{a,5}	V544 Lyr	HIDES	120	7.43	F0	A7 IV
184522 ^{a,5}	V2084 Cyg	HIDES	100	7.34	A3	F2 IV
453111 ^{a,5}	V456 Aur	HIDES	80	7.85	F0	F2 III

*High-amplitude δ Sct stars (HADS); **star of intermediate amplitude variation (between HADS and low-amplitude δ Sct stars (LADS) (Chang et al. 2013). ^aSuspected δ Sct stars. ¹Plume & Percy (1988), ²Schutt (1991), ³Schutt (1993), ⁴Hao & Huang (1995), ⁵Kazarovets et al. (1999), ⁶Duerbeck (1997)

greater than 100 parsec. The Gaia parallaxes are more accurate for the distances greater than 100 parsec. For the member of Pleiades cluster V624 Tau, we used the cluster distance to calculate the $E(B - V)$, because the parallax of this star has not been measured. The errors of $E(B - V)$ mainly come from the uncertainty of targets' distances. The largest error of $E(B - V)$ value was found to be 0.08 mag. In the second method, we calculated $E(B - V)$ values from $uvby\beta$ photometry. The $E(b - y)$ values were firstly calculated utilizing the method of Moon & Dworetzky (1985). Using the transformation $E(B - V) = 1.4 E(b - y)$ (Cardelli, Clayton, & Mathis 1989), the $E(B - V)$ values were found and the average error of these $E(B - V)$ values was obtained to be 0.02 mag. In the last method,

the $E(B - V)$ was derived by using the relation between equivalent width of Na D₂ line (5889.95 Å) and $E(B - V)$ (Munari & Zwitter 1997). In this method uncertainties of the $E(B - V)$ values were adopted to be 0.02 mag (Kahraman Aliçavuş et al. 2016) (hereafter KA16). The obtained $E(B - V)$ values are listed in Table 3. As can be seen, $E(B - V)$ determined with all methods are generally in agreement with each other within error bars. In the photometric analysis, the more accurate $E(B - V)$ values determined from the Na D₂ line were used.

In the next step, the atmospheric parameters, T_{eff} and $\log g$, were derived using the de-reddened indices of Johnson, 2MASS, $uvby\beta$ Strömrgren and Geneva photometric systems. The photometric data were gath-

Table 3. The interstellar reddening $E(B - V)$ and derived atmospheric parameters from photometric indices and SED analysis.

HD number	Name	$E(B-V)_{uvby\beta}$ (mag)	$E(B-V)_{Map}$ (mag)	$E(B-V)_{NaD_2}$ (mag)	$T_{\text{eff}}_{uvby\beta}$ (K) ± 95	$\log g_{uvby\beta}$ ± 0.10	T_{eff}_{Geneva} (K) ± 125	$\log g_{Geneva}$ ± 0.11	T_{eff}_{UBV} (K) ± 170	T_{eff}_{2MASS} (K) ± 80	T_{eff}_{SED} (K)
089843	EN UMa	0.00	0.01	0.00	7260	3.29			7560	7260	7245 \pm 120
099002	CX UMa	0.00	0.01	0.00	7500	3.65	7480	4.08	7410	7400	7550 \pm 150
115308	DK Vir	0.00	0.00	0.00	6960	3.44	6960	3.86	7100	6955	7110 \pm 100
	EH Lib		0.02	0.00					7440	7250	7235 \pm 100
010088		0.00	0.03	0.00	7310	4.02	7480	4.38	7050	7340	7000 \pm 150
012389		0.08	0.04	0.05	8230	3.82			8050	7820	8300 \pm 250
023156	V624 Tau	0.04	0.03	0.01	7970	4.25	7700	4.47	7400	7400	7720 \pm 180
062437	AZ CMi	0.01	0.01	0.00	7820	3.61	7700	3.81	7785	7575	7420 \pm 150
073857	VZ Cnc	0.00	0.02	0.01	6450	2.86	7000	3.78	7210	7170	7190 \pm 210
103313	IQ Vir	0.02	0.01	0.01	7870	3.68	7695	3.84	7785	7585	7460 \pm 130
110377	GG Vir	0.00	0.00	0.00	7720	3.89	7790	4.26	7850	7630	7800 \pm 110
191635	V2109 Cyg	0.01	0.06	0.09	7130	3.47			7210	7200	7260 \pm 150
192871	V383 Vul	0.03	0.02	0.02	7130	3.44			7215	6920	7300 \pm 140
199908	DQ Cep	0.00	0.01	0.00	7130	3.56	6940	3.74	7100	7030	7260 \pm 100
210957		0.02	0.01	0.01	7870	3.80			7560	7670	7600 \pm 100
213272		0.00	0.01	0.00	9100	4.07	9185	4.16	9000		9115 \pm 130
214698	41 Peg	0.00	0.05	0.05	9113	3.69	9840	3.93	9480		9445 \pm 160
219586	V388 Cep		0.01	0.00					7490	7235	7190 \pm 210
034409	BS Cam	0.09	0.10	0.06	6995	3.22			6950	6900	7360 \pm 270
037819	V356 Aur	0.14	0.14	0.09	6780	3.78	6450	2.84	6660	6670	6800 \pm 220
050018	OX Aur	0.02	0.01	0.00	6810	3.44			6870	6730	6840 \pm 145
060302	V344 Gem	0.00	0.01	0.00	7310	3.78			7430	7170	7200 \pm 130
079781	GG UMa	0.00	0.09	0.06	6930	3.84			6900	6970	6930 \pm 200
081882	KZ UMa	0.00	0.05	0.01	7220	3.55			7270	7470	7810 \pm 130
082620	DL UMa	0.00	0.01	0.00	7175	3.74			7100	7265	7460 \pm 140
084800	IX UMa		0.02	0.00					8650		8760 \pm 190
090747	GS UMa		0.04	0.01					6550	6430	6610 \pm 120
093044	EO UMa	0.00	0.01	0.01	7230	3.83	7270	4.18	7380	7190	7380 \pm 240
097302	FI UMa	0.01	0.02	0.02	8500	4.19	8850	4.35	8755		8870 \pm 120
099983	HQ UMa	0.01	0.03	0.01	7145	3.52			7160	7030	7300 \pm 100
102355	KW UMa	0.00	0.03	0.01	7550	3.71			7710	7460	7900 \pm 160
118954	IP UMa	0.04	0.01	0.01	7510	3.79			7240	7200	7550 \pm 130
127411	IT Dra		0.00	0.01					8270	8100	7940 \pm 110
151938	V919 Her		0.01	0.00					7185	7105	7015 \pm 100
154225	V929 Her	0.00	0.01	0.01	6950	3.90			6480	6780	7130 \pm 250
155118	V873 Her	0.06	0.02	0.05	7190	3.66			7160	7030	7120 \pm 200
161287	V966 Her	0.00	0.02	0.02	7110	3.68			7160	7170	7500 \pm 270
176445	V1438 Aql	0.09	0.02	0.07	7015	3.48			6850	6860	7150 \pm 120
176503	V544 Lyr	0.06	0.02	0.02	7900	3.60			7360	7410	7700 \pm 160
184522	V2084 Cyg		0.01	0.01					7030	7090	6895 \pm 100
453111	V456 Aur	0.04	0.02	0.03	6970	3.67			7030	6860	7150 \pm 200

ered from the General Catalogue of photometric data (GCPD⁵) (Mermilliod, Mermilliod, & Hauck 1997), the 2MASS catalogue (Cutri et al. 2003), and the updated catalogue of Strömgren-Crawford $uvby\beta$ photometry (Paunzen 2015). The T_{eff} and $\log g$ parameters were derived using the methods described by Moon & Dworetzky (1985), Künzli et al. (1997), Sekiguchi & Fukugita (2000) and Masana, Jordi, & Ribas (2006) for the Strömgren, Geneva, Johnson and 2MASS systems, respectively. The T_{eff} parameters were determined using all mentioned photometric systems, while $\log g$ parameters were obtained from Strömgren and Geneva photometric systems only. In the calculations of T_{eff} from Johnson, and 2MASS photometry, $\log g = 4.0$ and solar metallicity were assumed. The uncertainties of de-

termined T_{eff} and $\log g$ parameters were calculated taking into account errors of $E(B - V)$ and used indices. It turned out that the error on $E(B - V)$ contributes most to the uncertainty ($\sim 90\%$). The calculated atmospheric parameters and their uncertainties are given in Table 3.

In the last step, the T_{eff} parameters were determined by using SED. In the analysis, the code written by Dr. Shulyak (private information) was used. The code automatically scans some spectrophotometric and photometric catalogues and offers the possibility to manually add some photometric data (for more information see KA16). In these calculations, solar metallicity and $\log g = 4.0$ were fixed. Final parameters are derived by comparing input data with the calculated theoretical spectra (Kurucz 1993, ATLAS9 code). The obtained T_{eff} values and their errors are given in Table 3.

⁵ <http://obswww.unige.ch/gcpd/gcpd.html>

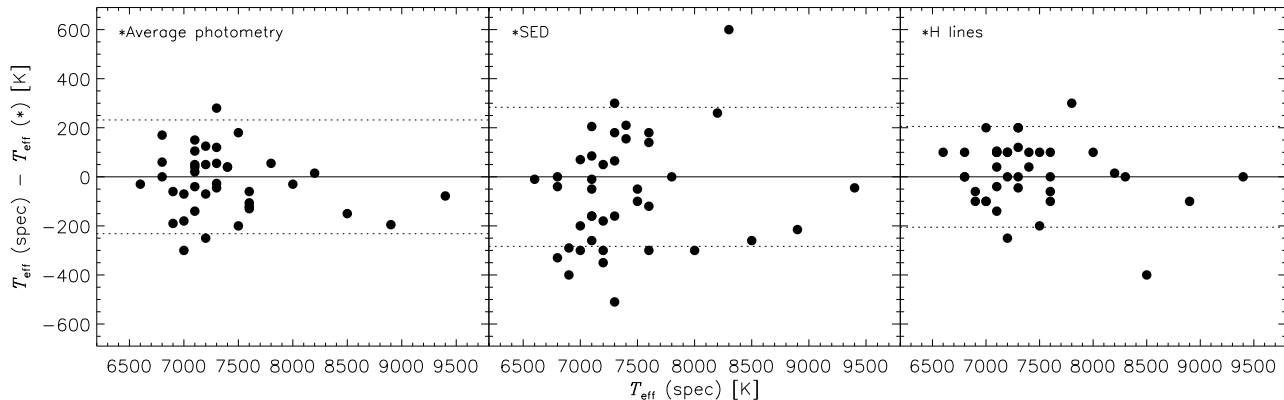


Figure 1. Comparison of spectroscopic T_{eff} values with the average photometric values, SED results and these from hydrogen lines analysis. The dotted lines represent 1- σ level.

5 SPECTROSCOPIC ATMOSPHERIC PARAMETERS AND CHEMICAL ABUNDANCE ANALYSIS

Stellar atmospheric parameters have been determined from Balmer and metal lines analysis. Atmospheric chemical abundances were obtained using the spectral synthesis method. The hydrostatic, plane-parallel, and line-blanketed local thermodynamic equilibrium (LTE) atmosphere models were calculated with the ATLAS9 code (Kurucz 1993), whereas the synthetic spectra were obtained with the SYNTH3 code (Kurucz & Avrett 1981).

5.1 Analysis of Balmer lines

To obtain T_{eff} values, H β , H γ , and H δ lines were used. The HIDES spectra are in the range from 4080 to 7525 Å, hence the H δ line profiles were not used in their analysis. The procedure described by Catanzaro, Leone, & Dall (2004) was applied to derive T_{eff} values from the analysis of Balmer lines. For stars with initial T_{eff} lower than 8000 K, the $\log g$ values were adopted to be 4.0, as the Balmer lines are not sensitive to $\log g$ for such temperatures (Smalley et al. 2002; Smalley 2005). For stars with estimated T_{eff} values higher than 8000 K, both T_{eff} and $\log g$ were derived simultaneously. Additionally, metallicities of the stars were assumed to be 0.0 dex. The analysis was performed separately for each Balmer line. Final averaged T_{eff} and $\log g$ (for stars with $T_{\text{eff}} > 8000$ K) values are given in Table 4.

To estimate the uncertainties of T_{eff} and $\log g$ values determined from the Balmer lines analysis, we checked both, errors caused by the normalisation process and introduced by the assumed parameters such as $\log g$, metallicity, and $v \sin i$. The correct normalisation of Balmer lines is difficult, especially in the case of broad Balmer lines, which can be spread over more than one échelle order. The error of T_{eff} caused by inaccurate normalisation has been estimated as approximately 100 K by checking the standard deviation of the different Balmer line’s determinations. When we took into account the effects of wrongly assumed values of $\log g$, metallicity, and $v \sin i$, an average uncertainty of T_{eff} was found to be 200 K. The uncertainties of $\log g$ were obtained in a similar way, taking into account normalisation problems

and effects of assumed parameters. The total uncertainties of T_{eff} and $\log g$ parameters were obtained using the squared sum of the individual contributions. The obtained parameters and their uncertainties are given in Table 4.

5.2 Analysis of metal lines

The final atmospheric parameters, T_{eff} , $\log g$, and microturbulent velocities (ξ) were obtained using the neutral and ionised iron lines. Previously determined atmospheric parameters were used as input values. The analysis was performed in the following steps:

- The normalised spectra were divided into shorter spectral parts taking into account $v \sin i$ values of the stars. For fast rotating objects ($v \sin i > 100 \text{ km s}^{-1}$) long parts covering many blended spectral lines were analysed, whereas for slowly rotating objects ($v \sin i < 30 \text{ km s}^{-1}$) short parts with one or few lines were taken into account.
- The line identification for each part was performed using the line list of Kurucz ⁶.
- Analysis of the metal lines was performed for a range of T_{eff} , $\log g$, and ξ by using the spectrum synthesis method. The detailed information about the method can be found in Niemczura & Połubek (2006). The analysis was carried out in steps of 100 K, 0.1, and 0.1 km s^{-1} for T_{eff} , $\log g$, and ξ , respectively.
- The atmospheric parameters were obtained using the excitation potential (for T_{eff}) and ionisation balance (for $\log g$) of neutral and ionised iron lines. The ξ parameters were derived checking the correlation between the iron abundances and depths of iron lines (for more details see KA16). Simultaneously, $v \sin i$ parameters were adjusted.

The final atmospheric parameters are listed in Table 4. The T_{eff} values derived from different photometries and SEDs were compared with the spectroscopic T_{eff} values in Fig. 1. As can be seen, these values are generally in agreement within 1- σ level. In Fig. 2, the distributions of the spectroscopic atmospheric parameters are presented.

⁶ kurucz.harvard.edu/linelists.html

The uncertainties of the spectroscopic atmospheric parameters were determined considering relations between the iron abundances and both, excitation potentials of neutral or ionised iron lines, and lines depths. For the accurate parameters, there is no correlation between them. It means that we have similar iron abundances, regardless of line excitation potential or line depth. To find the errors of T_{eff} , $\log g$, and ξ we check how these parameters change for correlation differences of about 5%. Using this method the maximum uncertainties of T_{eff} , $\log g$, and ξ were obtained to be 300 K, 0.3 dex, and 0.4 km s^{-1} , respectively.

After the determination of accurate atmospheric parameters, the abundance analysis was performed with the spectrum synthesis method. An example of fitting of the synthetic spectrum to the observed one is shown in Fig. 3 for the slowly rotating star HD 161287.

The $v \sin i$ values and the chemical abundances are shown in Table 4 and Table 5, respectively. The distribution of the $v \sin i$ values is given in Fig. 4. The obtained $v \sin i$ range from 10 to 222 km s^{-1} .

In Table 5 chemical abundances and their standard deviations are given for five analysed stars. The full table is given in the electronic form. The total errors of the determined abundances are due to the uncertainties of T_{eff} , $\log g$, ξ , and $v \sin i$, assumptions adopted to calculate atmospheric models and synthetic spectra, quality of the data (resolving power, S/N), and the normalisation of spectra.

The assumptions adopted in the atmospheric model calculations (e.g. LTE, plane-parallel geometry, and hydrostatic equilibrium) cause an error of about 0.1 dex in chemical abundances (Mashonkina 2011). The uncertainties due to the resolving power and the S/N ratio of a spectrum were examined by KA16 and Ryabchikova et al. (2016). KA16 found uncertainties of about 0.07 dex and 0.13 dex for the iron abundance, resulting from the resolving power difference ($R=67000$ and $R=80000$), and the S/N ratio difference ($S/N=310$ and $S/N=170$), respectively. In our study, such introduced uncertainties in chemical abundances cannot be checked, as we do not have even one star observed by different instruments. Therefore these uncertainties were adopted from KA16.

To find the uncertainties of chemical abundances introduced by possible errors in atmospheric parameters T_{eff} , $\log g$, and ξ , we have selected a few stars with effective temperatures typical for the analysed sample. We were changing values of their atmospheric parameters to check how such changes will influence the determined abundances of chemical elements. If the error of T_{eff} equals 100 K, the abundance of iron will change of 0.05 dex. Smaller differences, 0.01 and 0.02 dex, are caused by the 0.1 error of $\log g$ and the 0.1 km s^{-1} uncertainty of ξ . The $v \sin i$ effect on chemical abundances was examined as well. We found that the uncertainties in abundances caused by $v \sin i$ are in a range of 0.05 – 0.25 dex. The higher error values were obtained for stars with the higher $v \sin i$ values.

The combined errors calculated taking into account all mentioned effects are given in Table 4 for the iron abundances.

6 DISCUSSION OF THE RESULTS

6.1 Atmospheric parameters of δ Sct stars

The T_{eff} range of investigated δ Sct stars was found to be 6600–9400 K. The typical T_{eff} values of δ Sct stars vary from 6300 to 8600 K (Uytterhoeven et al. 2011). As can be seen, the derived T_{eff} range is in agreement with the characteristic T_{eff} values of δ Sct stars. However, there are two hot stars (HD 213272 and HD 214698) that are located beyond the T_{eff} range. These stars are suspected δ Sct variables (see Table 2) and the nature of their variability should be checked.

We compared the determined range and average values of T_{eff} for δ Sct stars with those for γ Dor's obtained by KA16. The average T_{eff} ($\sim 7440 \pm 260 \text{ K}$) of δ Sct stars is slightly higher than this calculated for γ Dor's ($7060 \pm 130 \text{ K}$), as expected. However, T_{eff} ranges of both variables overlap. This gives us an opportunity to check whether there is a chemical difference between both types of pulsating stars located in the same area of H-R diagram, close to the blue edge of the γ Dor instability strip (see Sect. 6.4).

The distribution of $\log g$ determined from the iron lines analysis is shown in the middle panel of Fig. 2. The $\log g$ values were found between 3.4 and 4.3. The obtained $\log g$ values are in good agreement with the luminosity range (V-III) of δ Sct stars. Previous studies of δ Sct stars (e.g. Fossati et al. 2008; Catanzaro et al. 2011) give $\log g$ between 3.0 and 4.3 which are also in agreement with our results. For γ Dor stars $\log g$ ranges from 3.8 to 4.5 (KA16). It seems that δ Sct stars are more evolved than γ Dor stars, as expected.

The distribution of the derived ξ is shown in the right-hand panel of Fig. 2. The ξ ranges from 1.2 to 4.0 km s^{-1} with the average value $2.73 \pm 0.23 \text{ km s}^{-1}$. The ξ values for γ Dor stars were found in the range from 1.3 to 3.2 km s^{-1} with the average value $2.25 \pm 0.2 \text{ km s}^{-1}$ (KA16). The ξ values of δ Sct stars are higher than determined for γ Dor stars within errors. It is consistent with the relation between the ξ and T_{eff} (see e.g. Niemczura et al. 2015, and references therein). This relation was examined by Landstreet et al. (2009), Gebran et al. (2014), Niemczura et al. (2015) and KA16. It turned out that the ξ value is inversely proportional to T_{eff} for T_{eff} higher than $\sim 7400 \text{ K}$. This relation for our stars is shown in Fig. 5. As can be seen from the figure, there is no difference between microturbulence values for CP and normal stars. Similar results were found by Niemczura et al. (2015) and KA16.

The $v \sin i$ values of the analysed stars range from 10 to 222 km s^{-1} , with the average value $88 \pm 5 \text{ km s}^{-1}$. According to the previous studies (Fossati et al. 2008; Royer 2009; Catanzaro et al. 2011; Chang et al. 2013; Niemczura et al. 2015), the $v \sin i$ values of A-F stars are in a range from ~ 4 to 300 km s^{-1} . Our results are in agreement with the $v \sin i$ distributions given in the literature. The $v \sin i$ values of γ Dor stars are from 5 to 240 km s^{-1} and the average value is $81 \pm 3 \text{ km s}^{-1}$ (KA16), similar to these obtained for δ Sct stars.

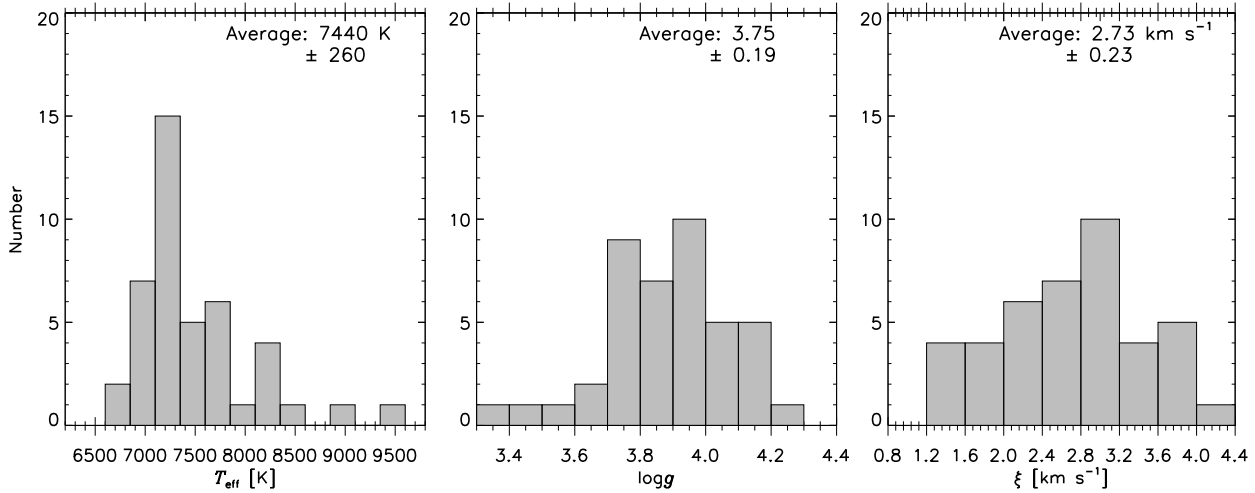


Figure 2. Distributions of the atmospheric parameters of the analysed δ Sct stars.

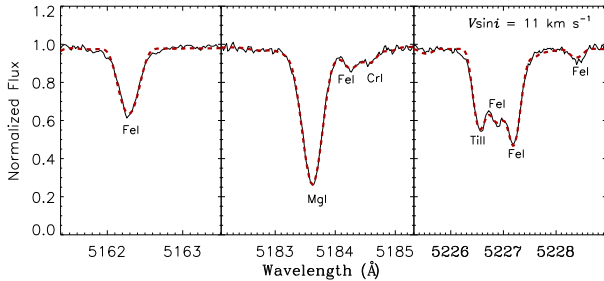


Figure 3. Comparison of the theoretical (dashed line) and observed spectra (continuous line) of HD 161287, one of the slowest rotating stars in our sample.

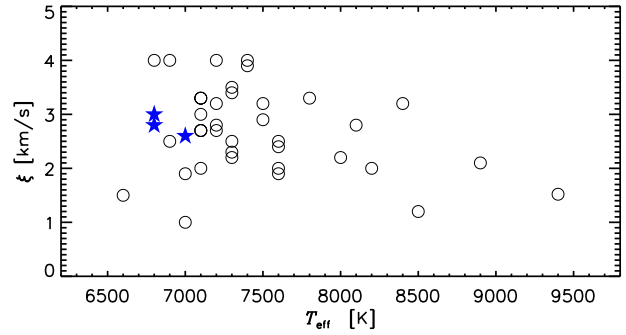


Figure 5. ξ as a function of T_{eff} . The star symbol represents the chemically peculiar objects.

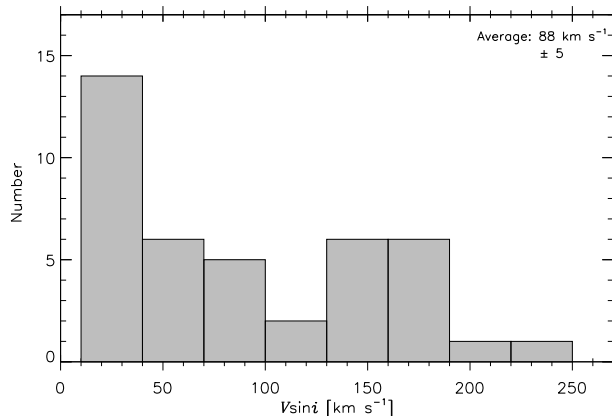


Figure 4. Distribution of $v \sin i$ values of stars.

6.2 Correlations between the atmospheric and pulsation parameters of δ Sct stars

The possible correlations between the pulsation quantities (pulsation period P_{puls} and amplitude Amp) and the obtained parameters were examined. For this purpose, the P_{puls} of the highest Amp and these Amp values in V -band were taken from

Rodríguez, López-González, & López de Coca (2000). Four high-amplitude δ Sct stars (HADS)⁷ are available in our sample. These stars were discarded in the following analysis. All the other objects represent typical Amp values of classical δ Sct stars.

In Fig. 6, the relations between T_{eff} and pulsation quantities are shown. As can be seen, there is an obvious correlation between T_{eff} and P_{puls} and Amp . These pulsation parameters have lower values for the hotter δ Sct stars. As known, changes in T_{eff} are related to the stellar radii (R) and the changes in R determine the position of helium ionisation zone which drives the δ Sct type pulsations (Cox 1980). Additionally, this negative correlation between P_{puls} and T_{eff} can be explained taking into account basic equations. Using the luminosity (L) – mass (M) relation ($L/L_{\odot} \approx M/M_{\odot}$), the mean density ($\bar{\rho} \sim M/R^3$), and the pulsation constant ($Q = P_{\text{puls}}(\bar{\rho}/\bar{\rho}_{\odot})^{0.5}$), we can obtain that $P_{\text{puls}} \propto (R/R_{\odot})^{0.5} (T_{\text{eff}}/T_{\text{eff}\odot})^{-2}$. Breger (1990) also showed that the P_{puls} depends on $\log g$, T_{eff} , and the bolometric magnitudes of pulsation stars. Balona & Dziembowski (2011) found similar relationships between P_{puls} , Amp and T_{eff} for δ Sct stars in the *Kepler* field. The $T_{\text{eff}} - P_{\text{puls}}$ relation was

⁷ The stars are signed in Table 2.

Table 4. Atmospheric parameters derived from Balmer and iron line analysis.

HD number	Name	Balmer lines		$\log g$	Fe lines		
		T_{eff} (K)	T_{eff} (K)		ξ (km s $^{-1}$)	$v \sin i$ (km s $^{-1}$)	$\log \epsilon$ (Fe)
089843	EN UMa	7300 \pm 300	7400 \pm 300	4.0 \pm 0.2	4.0 \pm 0.4	175 \pm 10	7.30 \pm 0.68
099002	CX UMa	7200 \pm 300	7200 \pm 200	4.2 \pm 0.2	4.0 \pm 0.3	145 \pm 6	7.38 \pm 0.62
115308	DK Vir	6800 \pm 300	7100 \pm 200	4.0 \pm 0.2	2.7 \pm 0.2	75 \pm 3	7.66 \pm 0.56
	EH Lib	7100 \pm 200	7300 \pm 100	3.9 \pm 0.1	2.5 \pm 0.2	15 \pm 1	7.11 \pm 0.45
010088		7100 \pm 200	7300 \pm 200	4.1 \pm 0.2	2.2 \pm 0.2	45 \pm 2	7.93 \pm 0.57
012389		7900 \pm 300	8000 \pm 200	3.8 \pm 0.2	2.2 \pm 0.3	85 \pm 5	7.11 \pm 0.65
023156	V624 Tau	7600 \pm 200	7600 \pm 200	4.0 \pm 0.1	1.9 \pm 0.1	35 \pm 3	7.63 \pm 0.50
062437	AZ CMi	7500 \pm 200	7600 \pm 100	3.9 \pm 0.1	2.4 \pm 0.2	42 \pm 3	7.56 \pm 0.45
073857	VZ Cnc	7000 \pm 200	6900 \pm 200	3.4 \pm 0.2	2.5 \pm 0.1	26 \pm 1	7.34 \pm 0.54
103313	IQ Vir	7700 \pm 200	7600 \pm 200	4.0 \pm 0.2	2.5 \pm 0.2	64 \pm 3	7.63 \pm 0.42
110377	GG Vir	7500 \pm 300	7800 \pm 200	3.8 \pm 0.2	3.3 \pm 0.3	173 \pm 5	7.18 \pm 0.63
191635	V2109 Cyg	6800 \pm 200	7100 \pm 200	3.8 \pm 0.2	3.0 \pm 0.2	15 \pm 3	7.67 \pm 0.51
192871	V383 Vul	7000 \pm 300	6900 \pm 100	3.8 \pm 0.2	4.0 \pm 0.3	148 \pm 5	7.23 \pm 0.36
199908	DQ Cep	7000 \pm 200	7100 \pm 200	3.8 \pm 0.1	2.7 \pm 0.1	64 \pm 3	7.82 \pm 0.41
210957		7700 \pm 300	7500 \pm 200	3.8 \pm 0.1	2.9 \pm 0.2	77 \pm 3	7.25 \pm 0.48
213272		9000 \pm 300*	8900 \pm 200	3.9 \pm 0.2	2.1 \pm 0.3	133 \pm 3	7.09 \pm 0.55
214698	41 Peg	9400 \pm 200*	9400 \pm 200	3.7 \pm 0.2	1.2 \pm 0.3	34 \pm 2	7.70 \pm 0.40
219586	V388 Cep	7300 \pm 300	7400 \pm 200	4.0 \pm 0.2	3.9 \pm 0.3	169 \pm 5	7.33 \pm 0.57
034409	BS Cam	7000 \pm 300	6900 \pm 200	3.5 \pm 0.3	2.5 \pm 0.3	197 \pm 10	7.81 \pm 0.74
037819	V356 Aur	6700 \pm 300	6900 \pm 200	4.0 \pm 0.2	3.1 \pm 0.2	24 \pm 2	7.89 \pm 0.48
050018	OX Aur	6800 \pm 300	6800 \pm 300	3.6 \pm 0.2	4.1 \pm 0.3	155 \pm 12	7.33 \pm 0.68
060302	V344 Gem	7000 \pm 300	7300 \pm 200	4.0 \pm 0.2	2.2 \pm 0.3	143 \pm 5	7.51 \pm 0.69
079781	GG UMa	6700 \pm 300	6900 \pm 200	4.1 \pm 0.2	2.9 \pm 0.3	64 \pm 3	7.59 \pm 0.56
081882	KZ UMa	7400 \pm 300	7200 \pm 300	3.7 \pm 0.3	3.7 \pm 0.2	117 \pm 5	7.27 \pm 0.53
082620	DL UMa	7200 \pm 300	7400 \pm 200	4.2 \pm 0.1	3.6 \pm 0.2	68 \pm 2	7.44 \pm 0.54
084800	IX UMa	8200 \pm 300*	8400 \pm 200	4.2 \pm 0.2	1.3 \pm 0.3	167 \pm 7	7.60 \pm 0.62
090747	GS UMa	6300 \pm 200	6600 \pm 300	4.0 \pm 0.2	1.5 \pm 0.2	34 \pm 2	7.41 \pm 0.57
093044	EO UMa	7200 \pm 300	7100 \pm 200	3.9 \pm 0.2	2.9 \pm 0.3	113 \pm 4	7.15 \pm 0.60
097302	FI UMa	7600 \pm 300	8100 \pm 300	4.2 \pm 0.2	3.3 \pm 0.3	132 \pm 6	7.69 \pm 0.75
099983	HQ UMa	6800 \pm 300*	7000 \pm 200	4.3 \pm 0.2	1.2 \pm 0.2	161 \pm 8	7.84 \pm 0.64
102355	KW UMa	8000 \pm 300	7600 \pm 300	3.8 \pm 0.3	2.0 \pm 0.4	175 \pm 17	7.22 \pm 0.77
118954	IP UMa	7000 \pm 200	7500 \pm 200	3.9 \pm 0.1	3.1 \pm 0.2	26 \pm 2	7.64 \pm 0.48
127411	IT Dra	8100 \pm 300*	8100 \pm 200	4.1 \pm 0.2	2.0 \pm 0.4	222 \pm 9	7.19 \pm 0.72
151938	V919 Her	7000 \pm 200	7200 \pm 100	3.8 \pm 0.2	1.7 \pm 0.2	10 \pm 1	7.72 \pm 0.44
154225	V929 Her	6800 \pm 200	6900 \pm 200	3.9 \pm 0.2	2.9 \pm 0.2	35 \pm 2	7.61 \pm 0.49
155118	V873 Her	7100 \pm 300	7300 \pm 200	3.9 \pm 0.2	2.3 \pm 0.2	70 \pm 3	7.76 \pm 0.51
161287	V966 Her	7000 \pm 200	7100 \pm 200	4.0 \pm 0.1	3.1 \pm 0.1	11 \pm 1	7.31 \pm 0.48
176445	V1438 Aql	7100 \pm 300	7200 \pm 200	4.0 \pm 0.2	2.9 \pm 0.2	94 \pm 5	7.54 \pm 0.62
176503	V544 Lyr	7600 \pm 200	8100 \pm 200	3.8 \pm 0.2	2.8 \pm 0.2	10 \pm 1	7.94 \pm 0.50
184522	V2084 Cyg	6700 \pm 200	7100 \pm 200	4.1 \pm 0.2	3.2 \pm 0.2	37 \pm 3	7.51 \pm 0.51
453111	V456 Aur	7000 \pm 200	7100 \pm 200	4.1 \pm 0.1	3.3 \pm 0.1	24 \pm 1	7.22 \pm 0.49

* $\log g$ values were determined from Balmer lines' analysis: HD 213272: $\log g = 4.0 \pm 0.1$, HD 214698: $\log g = 3.7 \pm 0.1$, HD 84800: $\log g = 3.8 \pm 0.2$, HD 102355: $\log g = 3.6 \pm 0.1$, HD 127411: $\log g = 4.0 \pm 0.3$.

also found for δ Sct stars in eclipsing binaries (Kahraman Aliçvuş et al., in preparation). The same relations for γ Dor stars were checked by KA16. They did not find any significant correlation between T_{eff} and Amp , while a weak and negative correlation was found between T_{eff} and P_{puls} . This weak correlation is probably caused by the narrow T_{eff} range of the analysed γ Dor stars which were used to check relations (from 6900 to 7300 K).

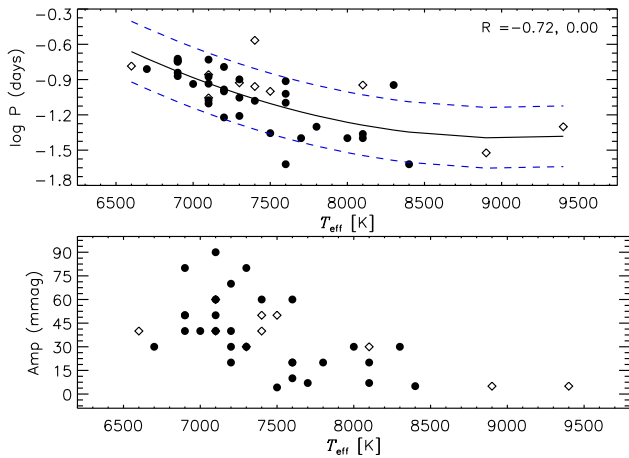
The correlations of $\log g$ values with the pulsation quantities were examined as well. The suitable relations are shown in the Fig. 7. As can be seen, there are no significant correlations between $\log g$, P_{puls} and Amp . On the other hand, Claret et al. (1990) and Breger (1990) found a relation between P_{puls} and $\log g$. According to them, P_{puls} decreases with increasing $\log g$ values. δ Sct stars in our study were selected considering their positions in the $\log g - \log T_{\text{eff}}$ di-

agram. Most stars in our sample have $\log g$ values from 3.8 to 4.2. Only three stars have $\log g$ below 3.6 and the P_{puls} values for them are clearly higher than the average period of stars with higher $\log g$ values. So, the chosen sample of stars can be the reason why the $\log g - P_{\text{puls}}$ is not observed. The same relation was examined for γ Dor stars by KA16 and a weak and negative correlation was found between $\log g$ and Amp , while no correlation was found between $\log g$ and P_{puls} .

Next, the possible correlations of ξ values with the pulsation quantities were checked. These relations are demonstrated in Fig. 8. As can be seen, there are no significant correlations between ξ and pulsation quantities. In general, higher values of P_{puls} correspond to higher values of ξ . The same correlation were examined in KA16 for γ Dor stars.

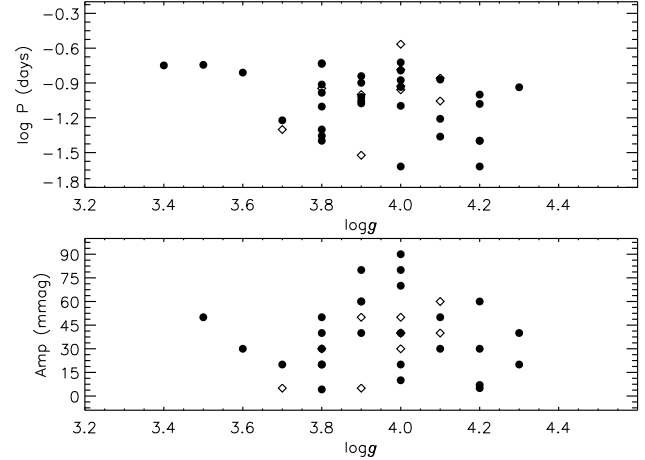
Table 5. Average abundances and standard deviations of individual elements. Number of the analysed spectral parts is given in the brackets. The full table is available in the electronic form.

Elements (atomic number)	HD 89843	HD 99002	HD 115308	HD 10088	HD 23156
C (6)	8.99 ± 0.21 (2)	8.71 ± 0.20 (2)	8.83 ± 0.24 (4)	7.92 ± 0.32 (3)	8.156 ± 0.15 (4)
N (7)					
O (8)	9.21 ± 0.21 (1)		8.97 ± 0.24 (1)	8.46 ± 0.32 (1)	8.97 ± 0.22 (1)
Na (11)			5.74 ± 0.24 (1)	7.18 ± 0.32 (2)	6.44 ± 0.22 (2)
Mg (12)	7.85 ± 0.21 (2)		7.81 ± 0.29 (5)	7.64 ± 0.14 (4)	8.10 ± 0.31 (5)
Si (14)	6.90 ± 0.21 (2)		6.93 ± 0.37 (9)	7.12 ± 0.52 (9)	7.21 ± 0.34 (10)
S (16)	7.63 ± 0.21 (2)		7.17 ± 0.24 (2)	7.69 ± 0.32 (1)	7.43 ± 0.22 (2)
Ca (20)	6.41 ± 0.34 (6)	6.03 ± 0.31 (8)	6.50 ± 0.19 (15)	5.71 ± 0.26 (12)	6.62 ± 0.19 (13)
Sc (21)	2.49 ± 0.21 (2)	3.28 ± 0.11 (3)	3.17 ± 0.17 (6)	1.95 ± 0.32 (3)	3.22 ± 0.15 (8)
Ti (22)	5.07 ± 0.15 (7)	5.20 ± 0.25 (15)	5.08 ± 0.20 (30)	5.21 ± 0.21 (23)	5.11 ± 0.26 (23)
V (23)	4.50 ± 0.21 (1)		4.42 ± 0.24 (2)	4.55 ± 0.32 (2)	4.239 ± 0.22 (2)
Cr (24)	5.45 ± 0.25 (7)	5.62 ± 0.16 (9)	5.38 ± 0.21 (18)	6.09 ± 0.18 (26)	5.82 ± 0.31 (39)
Mn (25)	5.49 ± 0.21 (1)	5.56 ± 0.20 (3)	4.90 ± 0.31 (25)	5.59 ± 0.21 (11)	5.25 ± 0.22 (5)
Fe (26)	7.30 ± 0.17 (18)	7.38 ± 0.17 (26)	7.25 ± 0.15 (67)	7.93 ± 0.21 (118)	7.63 ± 0.17 (117)
Co (27)					
Ni (28)	6.33 ± 0.14 (4)	6.14 ± 0.22 (9)	5.97 ± 0.16 (16)	6.94 ± 0.20 (16)	6.27 ± 0.21 (16)
Cu (29)					4.82 ± 0.22 (1)
Zn (30)		4.42 ± 0.20 (1)		4.86 ± 0.32 (2)	4.10 ± 0.22 (1)
Sr (38)			3.21 ± 0.24 (2)	3.80 ± 0.32 (2)	3.72 ± 0.22 (2)
Y (39)	3.21 ± 0.21 (2)	2.90 ± 0.17 (4)	2.25 ± 0.43 (3)	3.58 ± 0.32 (2)	2.59 ± 0.22 (2)
Zr (40)	3.33 ± 0.21 (1)	3.16 ± 0.20 (1)	2.63 ± 0.24 (3)	3.00 ± 0.32 (2)	2.98 ± 0.22 (2)
Ba (56)	1.94 ± 0.21 (2)		2.85 ± 0.24 (2)	3.82 ± 0.32 (2)	2.11 ± 0.22 (2)

**Figure 6.** Correlations between T_{eff} and pulsation quantities. The solid and dashed lines in the upper panel show the correlation and $1\text{-}\sigma$ level. Circles and diamonds represent known and suspected δ Sct stars, respectively. R is spearman rank of the correlation, while the secondnumber represents deviations of points from the correlations.

They found that a positive relation between P_{puls} and ξ can occur.

The relations between $v \sin i$ and pulsation quantities are shown in Fig.9. As can be seen, there are no significant correlations. A weak negative correlation may exist for $v \sin i$ and Amp . Similar relations between $v \sin i$ and P_{puls} were also found in the literature (e.g. Rodríguez, López-González, & López de Coca 2000; Breger 2000; Tkachenko et al. 2013). For γ Dor stars a strong correlation between $v \sin i$ and P_{puls} and a weak correlation be-

**Figure 7.** The relations between pulsation quantities and $\log g$. Circles and diamonds represent known and suspected δ Sct stars, respectively.

tween $v \sin i$ and Amp were found as well (Van Reeth et al. (2015), KA16).

Relations between the metallicity and pulsation quantities are presented in Fig. 10. No correlations were found. However, the stars generally have metallicities lower than the solar one. There is no significant difference between the average iron abundance of δ Sct (7.47 dex) and γ Dor (7.41 dex) stars (KA16).

6.3 Positions of δ Sct stars in the $\log T_{\text{eff}} - \log g$ diagram

Positions of δ Sct stars in the $\log T_{\text{eff}} - \log g$ diagram have been examined in detail since new δ Sct stars have been dis-

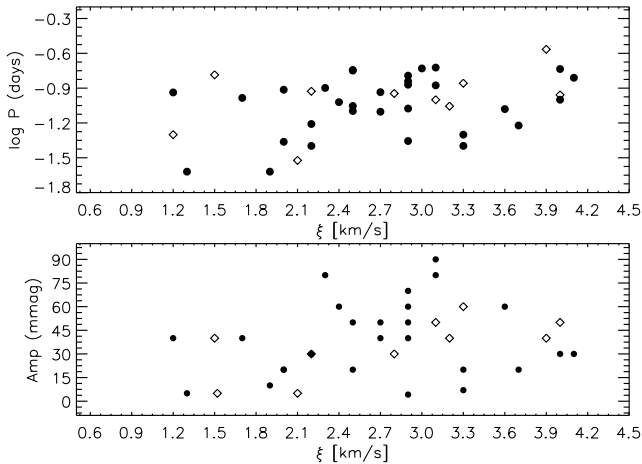


Figure 8. The relations between the pulsation quantities and ξ . Circles and diamonds represent known and suspected δ Sct stars, respectively.

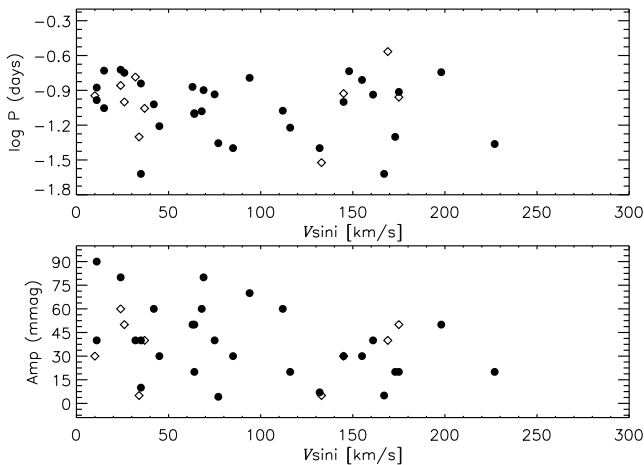


Figure 9. The relations between the pulsation quantities and $v \sin i$. Circles and diamonds represent known and suspected δ Sct stars, respectively.

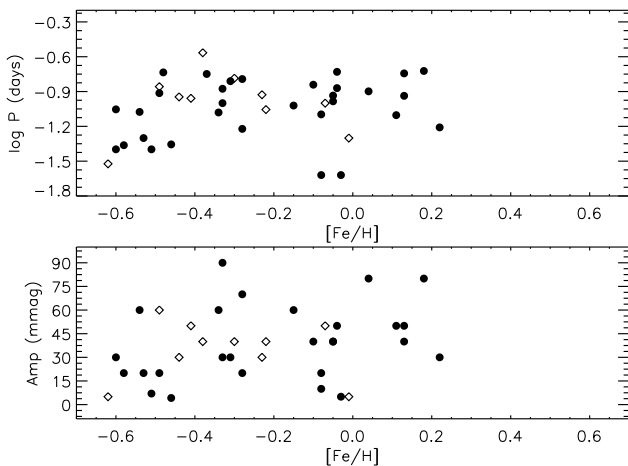


Figure 10. The relations between pulsation quantities and metallicity. Circles and diamonds represent known and suspected δ Sct stars, respectively.

covered by the space telescopes (*MOST* Walker et al. 2003, *CoRoT* Auvergne et al. 2009, *Kepler* Borucki et al. 2010). Uytterhoeven et al. (2011) showed positions of these variables in the $\log T_{\text{eff}} - \log g$ diagram mainly based on the photometric atmosphere parameters from the KIC catalogue (Brown et al. 2011). They found that *Kepler* δ Sct stars are located both in their instability strip and outside of it. In the most recent study (Niemczura et al. 2015) accurate parameters of a few δ Sct stars were obtained and some of them were found outside of their domain. However, the theory cannot explain this.

In Fig. 11 we show the positions of the analysed δ Sct stars in the $\log T_{\text{eff}} - \log g$ diagram. As can be seen, most stars are located inside the δ Sct instability strip. However, there are a few stars placed outside of the δ Sct instability strip. HD 213272 and HD 214698 are located beyond the blue edge, while HD 90747 is located outside the red edge. The stars beyond the blue edge have the lowest amplitudes (~ 5 mmag), while the star on the cold side of the δ Sct instability strip does not show differences in pulsation quantities in comparison with the other δ Sct stars considered. However, all these stars are suspected δ Sct variables (see Table 2) and the verification of their variability types is necessary.

The positions of CP stars in the $\log T_{\text{eff}} - \log g$ diagram were also shown. In a recent study, metallic stars with δ Sct pulsations were found in the T_{eff} range of 6900 – 7600 K (Smalley et al. 2017). T_{eff} of CP stars analysed here are also in this range (within error) and are located in the γ Dor instability strip.

6.4 Chemical abundances of δ Sct stars

During the spectral classification and abundance analysis, a few chemically peculiar stars were found. HD 37819, HD 79781 and HD 154225 have overabundant iron-peak and heavy elements (Zn, Sr, Zr, and Ba). The chemical abundance patterns of the discovered chemically peculiar stars are given in Fig 12.

We compared the chemical abundance pattern of δ Sct stars with the non-pulsating and γ Dor stars' patterns. Atmospheric parameters and chemical abundances of eighteen non-pulsating stars were taken from Niemczura et al. (2015). The stars used in the comparisons were analysed using exactly the same as in the present work. We divided δ Sct stars into two groups: one contains all analysed δ Sct stars and second contains stars located only in the γ Dor area ($7100 < T_{\text{eff}} < 7300$, KA16) to check whether there are any differences between their abundance patterns. The comparisons are shown in Fig. 13. It is clearly seen that δ Sct stars in γ Dor area and the other δ Sct stars have abundance patterns similar to γ Dor stars. However, abundance patterns of δ Sct and γ Dor stars show small differences in comparison with the abundance patterns of non-pulsating stars. The Na is overabundant in non-pulsating stars in comparison with δ Sct and γ Dor variables. Additionally, abundances of Si and Cu are slightly lower in δ Sct and γ Dor stars than in the non-pulsating stars. On the other hand, Fe abundances are similar in the investigated types of stars. When we compare the abundance patterns of δ Sct and γ Dor stars, it turned out that Zn abundance is lower in γ Dor stars than in δ Sct stars, and Sr abundance is higher in δ Sct stars than in the

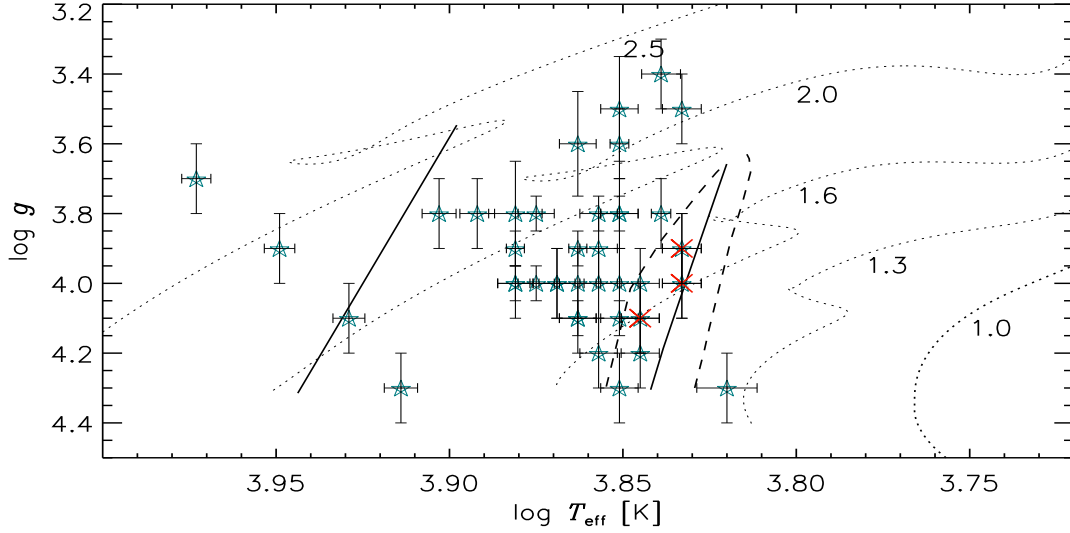


Figure 11. Positions of δ Sct stars in the theoretical instability strips of δ Sct (solid lines) and γ Dor stars (dashed-lines) (Dupret et al. 2005). Chemically peculiar stars are shown as crosses.

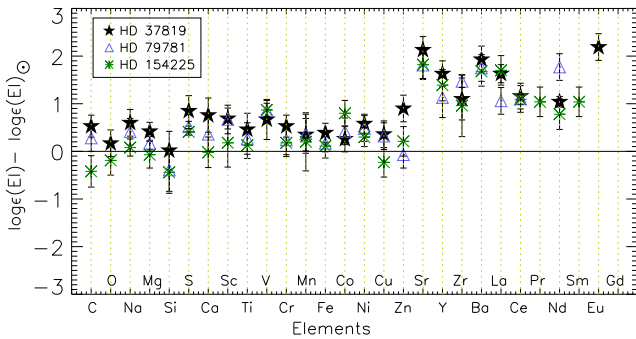


Figure 12. Chemical abundances of chemically peculiar stars compared with the solar values (Asplund et al. 2009).

non-pulsating and γ Dor stars. Fossati et al. (2008) found Y and Ba are over-abundant in δ Sct stars in comparison to the non-pulsating stars. However, we did not find any difference in abundances of these elements for δ Sct and non-pulsating stars.

7 CONCLUSIONS

This study presents the detailed spectroscopic investigation of a sample of 41 δ Sct stars. The initial atmospheric parameters (T_{eff} and $\log g$) were derived from the photometric indices, SED and Balmer lines. The accurate spectroscopic atmospheric parameters (T_{eff} , $\log g$ and ξ), $v \sin i$ values, and chemical abundances were obtained with the spectrum synthesis method.

T_{eff} and $\log g$ values of δ Sct stars were found in ranges of 6600–9400 K and 3.4–4.3, respectively. The $v \sin i$ values were derived from 10 to 222 km s⁻¹. Additionally, these parameters of δ Sct stars were compared with the parameters of γ Dor derived by KA16. As expected the average T_{eff} value of δ Sct stars is higher than the average T_{eff} value of γ Dor stars. We showed that δ Sct stars are more evolved than the

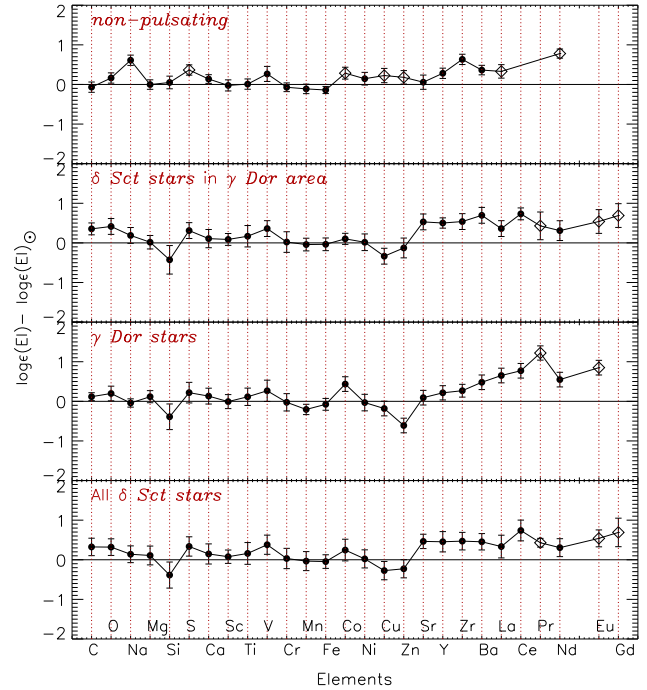


Figure 13. Comparisons of the chemical abundance patterns of δ Sct, γ Dor, and non-pulsating stars. The chemical abundances of γ Dor, non-pulsating stars and solar abundances were taken from Kahraman Aliçavuş et al. (2016); Niemczura et al. (2015) and Asplund et al. (2009), respectively. Filled circles and diamonds show values determined for more than 5 stars or less than 5 stars, respectively.

γ Dor stars. No significant difference was found between the average values and ranges of $v \sin i$.

The correlations between derived parameters and pulsation quantities were examined. As shown by Breger (1990), the P_{puls} varies depending on the $\log g$, T_{eff} , and bolometric magnitudes. In our study, we found that a strong correla-

tion between T_{eff} and P_{puls} exists. The $T_{\text{eff}} - P_{\text{puls}}$ correlation was also obtained for γ Dor stars (KA16) but this correlation was not as strong as for δ Sct stars. Additionally, although we did not find a significant $T_{\text{eff}} - \text{Amp}$ correlation, it is obvious that the hotter stars in our sample have the lowest Amp values. In the case of hotter stars, pulsation mechanism occurs very close to the stellar surface and it is not significantly effective to drive pulsations. This could explain the lower Amp values in hotter stars.

The $\log g - P_{\text{puls}}$ relation for pulsating stars has been known before (e.g. Claret et al. 1990; Breger 1990; Liakos & Niarchos 2017). However, because our sample consists of stars in a narrow $\log g$ range, we did not find relations between P_{puls} , Amp and $\log g$. Similarly, no correlation between ξ and P_{puls} was found for the analysed δ Sct stars. On the other hand, a weak positive correlation was obtained for γ Dor stars (KA16). Furthermore, the effect of $v \sin i$ on pulsation quantities was checked. Although a strong negative correlation between $v \sin i$ and P_{puls} was obtained for γ Dor stars in the previous study (KA16), the similar correlation was not obtained for δ Sct stars analysed here. The δ Sct stars pulsate in shorter periods and with higher Amp in comparison with the γ Dor stars. Because of the range of P_{puls} values of investigated δ Sct stars, the effect of $v \sin i$ on P_{puls} could not be obtained. Additionally, weak negative correlations between $v \sin i$ and Amp were found for both types of variables.

We examined the positions of δ Sct stars in $\log T_{\text{eff}} - \log g$ diagram and we conclude that most of our stars are located in δ Sct instability strip. Only three stars were found outside of their domain. The stars located beyond the blue edge of δ Sct domain, have the lowest Amp values in comparison with the other analysed variables. Additionally, some of investigated stars are placed in an overlapping area of δ Sct and γ Dor instability strips and the others are in δ Sct domain. When we compare pulsation properties of these two groups, we notice that the stars in overlapping area have higher Amp values. This result is in agreement with the $T_{\text{eff}} - \text{Amp}$ relation shown in Fig. 6. The stars in 7100 – 7300 K area have higher Amp values comparing the hotter ones.

Comparison of the abundance patterns of δ Sct, γ Dor, and non-pulsating stars were considered. We found that δ Sct stars have abundance pattern very similar to γ Dor stars. However, Na was obtained overabundant in non-pulsating stars in comparison with δ Sct and γ Dor stars, and Si, Cu were found underabundant in δ Sct and γ Dor stars in comparison with the non-pulsating ones. Additionally, Zn is slightly less abundant in γ Dor stars comparing with δ Sct stars, and Sr was obtained more abundant in δ Sct stars than in the non-pulsating and γ Dor stars. The Fe abundance was determined to be almost the same in all types of stars. The suggested chemical differences between δ Sct, γ Dor and non-pulsating stars can help us to understand why some stars in classical instability strip do not pulsate. However, such a chemical abundance comparison needs a bigger sample.

Accurate atmospheric parameters and chemical abundance patterns of δ Sct variables were derived. These parameters are important ingredients for a reliable seismic modelling of pulsating stars. Thus, the examination of the internal structure of stars in any evolutionary stage can be de-

rived more accurately. Additionally, obtained abundance differences between δ Sct, γ Dor, and non-pulsating stars may give us a first approach of understanding why some stars located in the classical instability strip do not show pulsations.

ACKNOWLEDGMENTS

The authors would like to thank the reviewer for useful comments and suggestions that helped to improve the publication. This work has been partly supported by the Scientific and Technological Research Council of Turkey (TUBITAK) grant numbers 2214-A and 2211-C. EN, MP, JMŽ and KH acknowledges support from the NCN grant No. 2014/13/B/ST9/00902. The calculations have been carried out in Wrocław Centre for Networking and Supercomputing (<http://www.wcss.pl>), grant No. 214. We are grateful to Dr. D. Shulyak for putting the code for calculating SEDs at our disposal. We thank to Dr. G. Catanzaro for putting the code for Balmer lines analysis at our disposal. This research has made use of the SIMBAD data base, operated at CDS, Strasbourg, France. This work has made use of data from the European Space Agency (ESA) mission Gaia (<http://www.cosmos.esa.int/gaia>), processed by the Gaia Data Processing and Analysis Consortium (DPAC, <http://www.cosmos.esa.int/web/gaia/dpac/consortium>). Funding for the DPAC has been provided by national institutions, in particular the institutions participating in the Gaia Multilateral Agreement.

REFERENCES

- Aerts C., Christensen-Dalsgaard J., Kurtz D. W., 2010, *Astroseismology*, Springer, Berlin
- Amôres E. B., Lépine J. R. D., 2005, *AJ*, 130, 659
- Aplund M., Grevesse N., Sauval A. J., Scott P., 2009, *ARA&A*, 47, 481
- Auvergne M., et al., 2009, *A&A*, 506, 411
- Balona L. A., Dziembowski W. A., 2011, *MNRAS*, 417, 591
- Balona L. A., 2014, *MNRAS*, 437, 1476
- Baranne A., et al., 1996, *A&AS*, 119, 373
- Borucki W. J., et al., 2010, *Sci*, 327, 977
- Breger M., Bregman J. N., 1975, *ApJ*, 200, 343
- Breger M., Beichbuchner F., 1996, *A&A*, 313, 851
- Breger M., 1990, *DSSN*, 2, 13
- Breger M., 2000, *ASPC*, 210, 3
- Brown T. M., Latham D. W., Everett M. E., Esquerdo G. A., 2011, *AJ*, 142, 112
- Cardelli J. A., Clayton G. C., Mathis J. S., 1989, *ApJ*, 345, 245
- Casertano S., Riess A. G., Bucciarelli B., Lattanzi M. G., 2017, *A&A*, 599, A67
- Catanzaro G., Leone F., Dall T. H., 2004, *A&A*, 425, 641
- Catanzaro G., et al., 2011, *MNRAS*, 411, 1167
- Chang S.-W., Protopapas P., Kim D.-W., Byun Y.-I., 2013, *AJ*, 145, 132
- Claret A., Rodriguez E., Rolland A., Lopez de Coca P., 1990, *ASPC*, 11, 481
- Cox, J. P. 1980, *Theory of Stellar Pulsation*, Princeton University Press, Princeton N.J., 1980.

- Cox A. N., 2000, *Allen's Astrophysical Quantities*,
 Cutri R. M., et al., 2003, 2MASS All Sky Catalog of point
 sources.
- Dekker H., D'Odorico S., Kaufer A., Delabre B., Kot-
 zowski H., 2000, SPIE, 4008, 534
- Duerbeck H. W., 1997, IBVS, 4513, 1
- Dupret M.-A., Grigahcène A., Garrido R., Gabriel M., Scu-
 flaire R., 2004, A&A, 414, L17
- Dupret M.-A., Grigahcène A., Garrido R., Gabriel M., Scu-
 flaire R., 2005, A&A, 435, 927
- Fossati L., Kolenberg K., Reegen P., Weiss W., 2008, A&A,
 485, 257
- Hao J., Huang L., 1995, A&A, 297, 754
- Handler G., Shobbrook R. R., 2002, MNRAS, 333, 251
- Heminiak K. G., Ukita N., Kambe E., Kozłowski S. K.,
 Sybilski P., Ratajczak M., Maehara H., Konacki M., 2016,
 MNRAS, 461, 2896
- Izumiura H., 1999, in: Proc. 4th East Asian Meeting on As-
 tronomy, ed. P. S. Chen, Kunming, Yunnan Observatory,
 p. 77
- Gray R. O., Corbally C. J., Garrison R. F., McFadden
 M. T., Robinson P. E., 2003, AJ, 126, 2048
- Gray R. O., Corbally C. J., 2009, *Stellar Spectral Classifi-
 cation*, Princeton University Press
- Gebran M., Monier R., Royer F., Lobel A., Blomme R.,
 2014, *Putting A Stars into Context: Evolution, Environ-
 ment, and Related Stars*, 193
- Grigahcène A., et al., 2010, ApJ, 713, L192
- Kahraman Aliçavuş F., et al., 2016, MNRAS, 458, 2307
- Kambe E., et al., 2013, PASJ, 65, 15
- Kazarovets E. V., Samus N. N., Durlevich O. V., Frolov
 M. S., Antipin S. V., Kireeva N. N., Pastukhova E. N.,
 1999, IBVS, 4659, 1
- Künzli M., North P., Kurucz R. L., Nicolet B., 1997, A&AS,
 122, 51
- Kurtz D. W., Saio H., Takata M., Shibahashi H., Murphy
 S. J., Sekii T., 2014, MNRAS, 444, 102
- Kurucz R. L., Avrett E. H., 1981, SAO Special Report,
 391,
- Kurucz R., 1993, ATLAS9 Stellar Atmosphere Programs
 and 2 km/s grid. Kurucz CD-ROM No. 13. Cambridge,
 Mass.: Smithsonian Astrophysical Observatory, 13,
- Kurucz R., Bell B., 1995, Atomic Line Data (R.L. Kurucz
 and B. Bell) Kurucz CD-ROM No. 23. Cambridge, Mass.:
 Smithsonian Astrophysical Observatory, 23,
- Landstreet J. D., Kupka F., Ford H. A., Officer T., Sigut
 T. A. A., Silaj J., Strasser S., Townshend A., 2009, A&A,
 503, 973
- Lehmann H., Southworth J., Tkachenko A., Pavlovski K.,
 2013, A&A, 557, A79
- Liakos A., Niarchos P., 2017, MNRAS, 465, 1181
- Masana E., Jordi C., Ribas I., 2006, A&A, 450, 735
- Mashonkina L., 2011, *Magnetic Stars*, 314
- Mayor M., Pepe, F., Queloz, D., et al., 2003, *The Messenger*,
 114, 20
- Mermilliod J.-C., Mermilliod M., Hauck B., 1997, A&AS,
 124, 349
- Miglio A., Montalbán J., Noels A., Eggenberger P., 2008,
 MNRAS, 386, 1487
- Moon T. T., Dworetzky M. M., 1985, MNRAS, 217, 305
- Moultaka J., Ilovaisky S. A., Prugniel P., Soubiran C., 2004,
 PASP, 116, 693
- Munari U., Zwitter T., 1997, A&A, 318, 269
- Niemczura E., Pohubek G., 2006, ESASP, 624, 120.1
- Niemczura E., Morel T., Aerts C., 2009, A&A, 506, 213
- Niemczura E., et al., 2015, MNRAS, 450, 2764
- Paunzen E., 2015, A&A, 580, A23
- Petersen J. O., Jørgensen H. E., 1972, A&A, 17, 367
- Plume R., Percy J. R., 1988, IBVS, 3225, 1
- Raskin G., et al., 2011, A&A, 526, A69
- Rodríguez E., López-González M. J., López de Coca P.,
 2000, A&AS, 144, 469
- Royer F., 2009, LNP, 765, 207
- Ryabchikova T., et al., 2016, MNRAS, 456, 1221
- Schutt R. L., 1991, AJ, 101, 2177
- Schutt R. L., 1993, PASP, 105, 22
- Sekiguchi M., Fukugita M., 2000, AJ, 120, 1072
- Smalley B., Gardiner R. B., Kupka F., Bessell M. S., 2002,
 A&A, 395, 601
- Smalley B., 2005, MSAIS, 8, 130
- Smalley B., et al., 2017, MNRAS, 465, 2662
- Tkachenko A., Lehmann H., Smalley B., Uytterhoeven K.,
 2013, MNRAS, 431, 3685
- Uytterhoeven K., Moya, A., Grigahcène A., Guzik, J. A.,
 Gutiérrez-Soto, J., et al., 2011, A&A, 534, AA125
- van Leeuwen F., 2007, A&A, 474, 653
- Van Reeth T., et al., 2015, ApJS, 218, 27
- Walker G., et al., 2003, PASP, 115, 1023
- Wenger M., et al., 2000, A&AS, 143, 9
- Zima W., Lehmann H., Stütz C., Ilyin I. V., Breger M.,
 2007, A&A, 471, 237